ANTIOXIDANTS & REDOX SIGNALING
Volume 7, Numbers 5 & 6, 2005

Forum Original Research Communication

Microarray Expression Profiling Identifies Early Signaling Transcripts Associated with 6-OHDA-Induced Dopaminergic Cell Death

WILLIAM A. HOLTZ, JAY M. TURETZKY, and KAREN L. O'MALLEY

ABSTRACT

The parkinsonian mimetic 6-hydroxydopamine (6-OHDA) has been shown to cause transcriptional changes associated with cellular stress and the unfolded protein response. As these cellular sequelae depend on upstream signaling events, the present study used functional genomics and proteomic approaches to aid in deciphering toxin-mediated regulatory pathways. Microarray analysis of RNA collected from multiple time points following 6-OHDA treatment was combined with data mining and clustering techniques to identify distinct functional subgroups of genes. Notably, stress-induced transcription factors such as ATF3, ATF4, CHOP, and C/EBPβ were robustly up-regulated, yet exhibited unique kinetic patterns. Genes involved in the synthesis and modification of proteins (various tRNA synthetases), protein degradation (*e.g.,* ubiquitin, Herpud1, Sqstm1), and oxidative stress (Hmox1, Por) could be subgrouped into distinct kinetic profiles as well. Real-time PCR and/or two-dimensional electrophoresis combined with western blotting validated data derived from microarray analyses. Taken together, these data support the notion that oxidative stress and protein dysfunction play a role in Parkinson's disease, as well as provide a time course for many of the molecular events associated with 6-OHDA neurotoxicity. *Antioxid. Redox Signal.* 7, 639–648.

INTRODUCTION

THE MECHANISMS behind the irreversible loss of dopaminergic neurons in the nigrostriatal pathway that results in Parkinson's disease (PD) remain undefined. Although recent findings have implicated genetic and environmental factors, these account for only a small percentage of cases. Postmortem studies of PD brains have provided evidence of a variety of abnormalities, most notably, evidence of increased oxidative stress, decreased mitochondrial function, inflammation, and aberrant protein degradation (1, 8, 19, 28). However, the pathways by which these factors lead to cell death and whether these factors are causative or a downstream symptom are unclear. In addition, the neurotransmitter dopamine itself is considered a major factor in PD pathology because it is easily oxidized into a variety of reactive metabolites (1, 6, 11, 29, 30). Both animal and cell culture models have been widely used to investigate possible mechanisms of cell death in dopaminergic neurons. Two of the most commonly studied models involve the neurotoxins, 1-methyl-4-phenylpyridinium (MPP^+) and 6-hydroxydopamine (6-OHDA) (1, 7). Both reagents are able to mimic some of the characteristics of PD, including motor impairment, selective loss of dopaminergic neurons, increased oxidative stress, inflammation, and energy impairment.

Earlier studies have shown that MPP^+ and 6-OHDA trigger morphologically distinct types of cell death in dopaminergic cells, although both depend on new protein synthesis (3, 4, 12, 15). Using microarray analysis to determine the underlying patterns of gene expression occurring in response to these parkinsonian mimetics, we previously reported that 6-OHDA triggered multiple signaling pathways associated with cellular stress and unfolded protein response, whereas MPP^+ seemed to activate a more limited stress response (15). Because these studies focused on transcriptional changes associated with the time point at which cells became committed to die, upstream signaling events would not have been detected.

Washington University School of Medicine, Anatomy and Neurobiology Department, St. Louis, MO.

In the present study, microarray experiments at earlier times were conducted to identify genetic events associated with initial 6-OHDA-mediated signaling cascades. Using a combination of data mining techniques, we have confirmed and extended our previous results showing that 6-OHDA activates cellular stress pathways via a common set of genes. Moreover, expression profile clustering has revealed additional, novel groups of genes involved in the death of dopaminergic cell types. Finally, real-time PCR and proteomic approaches have confirmed the ability of our microarray groupings to predict changes.

MATERIALS AND METHODS

Cell cultures and neurotoxin treatment

MN9D cells (2) were plated on dishes coated with 0.5 mg/ml poly-D-lysine (Sigma, St. Louis, MO, U.S.A.) for 1 h at 37°C and then rinsed with sterile water. Cells were maintained in Iscove's Dulbecco's modified Eagle's medium with 10% fetal bovine serum (Atlas, Fort Collins, CO, U.S.A.) in an incubator with 10% CO_2 at 37°C. Cells were switched to serum-free 1:1 Iscove's Dulbecco's modified Eagle's medium/Ham's F-12 supplemented with 1× B27 (Invitrogen, Carlsbad, CA, U.S.A.) prior to addition of 6-OHDA with ascorbic acid (Sigma). 6-OHDA was resuspended in water at a concentration of 20 m*M* before addition into cell culture medium.

Microarray analysis

MN9D cells were plated at a density of 200,000 cells/well in six-well plates. After 3 days, cells were treated with 75 μM 6-OHDA, or left untreated for control comparisons. Total RNA was isolated after 3 and 6 h of 6-OHDA treatment using an RNeasy kit (Qiagen, Valencia, CA, U.S.A.) according to the manufacturer's protocol. Equal amounts of total RNA from three independent experiments were pooled for each GeneChip hybridization. A minimum of 20 μg/sample of total RNA was sent to the Alvin J. Siteman Cancer Center GeneChip Core Facility (Washington University, St. Louis, MO, U.S.A.) for generation of labeled cRNA target and hybridization against Affymetrix Murine Genome U74Av2 GeneChip arrays (Santa Clara, CA, U.S.A.) using standard protocols (pathbox.wustl.edu/~mgacore/protocols.htm). Data were analyzed using Affymetrix Microarray Suite version 5.0. Data mining was performed using Spotfire Decision Site for Functional Genomics (Somerville, MA, U.S.A.). For those transcripts designated both "present" and "increasing" by the software, a threshold of a signal $\log_2$ ratio of 0.5 (~1.5-fold change) was set. Transcripts for which signal was <3% of the maximum signal were filtered out.

Real-time PCR analysis of gene expression

MN9D cells were plated and treated exactly as described for microarray experiments. Total RNA was isolated after 1, 2, 4, 6, 8, 10, and 12 h, as well as from untreated control. Reverse transcription of total RNA was done with AMV-RT (Promega, Madison, WI, U.S.A.) using gene-specific primers to generate cDNAs for use in real-time PCR analysis. Primer sequences used for quantitative analysis of each gene are available upon request. Real-time PCR analysis was performed with the ABI Prism 7000 Sequence Detection System (Applied Biosystems, Foster City, CA, U.S.A.) to determine the expression levels of selected genes. PCR product accumulation was monitored in real time by measuring the fluorescence of SYBR Green as described (21, 22). A standard curve of serial dilutions of cDNA from samples containing the highest expression of selected genes was used to determine relative expression levels. The average fold induction relative to control untreated cells was determined after normalizing to levels of glyceraldehyde-3-phosphate dehydrogenase (GAPDH). Standard deviation was obtained from three to six replicate measurements of each sample.

Two-Dimensional electrophoresis and western blot analysis

MN9D cells were plated and treated exactly as described for microarray experiments. Cell lysates were collected at 3, 6, 9, and 12 h following 75 μM 6-OHDA treatment and subjected to sodium dodecyl sulfate–polyacrylamide gel electrophoresis (SDS-PAGE) and western blot analysis as described previously (15). Two-dimensional electrophoresis was used to assess protein changes at 6 h following 75 μM 6-OHDA, 75 μM 6-OHDA plus 5 m*M* *N*-acetylcysteine (NAC), or 50 μM MPP^+ treatment, as well as untreated controls. Samples were prepared by lysing cells in 5% SDS, 5% β-mercaptoethanol, 10% glycerol, and 60 m*M* Tris, pH 6.8. Samples were then snap-frozen and shipped to Kendrick Labs (Madison, WI, U.S.A.) for two-dimensional electrophoresis and transblotting. Filters were subsequently probed in this laboratory using antibodies directed against heme oxygenase-1 (Hmox1, rabbit polyclonal, 1:5,000; StressGen, San Diego, CA, U.S.A.), CHOP (Ddit3/Gadd153) (mouse monoclonal, 1:100; Santa Cruz Biotechnology, Santa Cruz, CA, U.S.A.), and Hsp60 (goat polyclonal, 1:500; Santa Cruz Biotechnology). Anti-rabbit horseradish peroxidase-conjugated secondary antibody (1:2,000) was purchased from Cell Signaling Technologies (Beverly, MA, U.S.A.). Anti-mouse secondary (1:5,000) and anti-goat secondary (1:5,000) were from Sigma. Specific protein bands were detected by enhanced chemiluminescence substrate detection (ECL Plus; Amersham Biosciences, Piscataway, NJ, U.S.A.).

RESULTS

Microarray expression profiling

Previous microarray experiments revealed that 6-OHDA treatment increased the expression of many genes associated with cellular stress. Inasmuch as the prior studies looked only at a 9-h end point, the latest time that macromolecular synthesis inhibitors could block cell death (15), current studies were directed at establishing earlier hierarchical changes. In order to examine early toxin-induced changes in gene profiles, RNAs prepared from untreated control and 3- and 6-h 6-OHDA-treated cells were subjected to microarray analysis as described in Materials and Methods. Data from these experiments were combined with information from our prior 9-h time point to identify changes, generate expression profiles of transcriptional differences over time, and group genes according to

their profiles. In keeping with the ability of cycloheximide to block 6-OHDA-induced cell death (15), transcription was increased at all time points tested. Of the ~12,000 genes present on the GeneChip, the number of genes that met the criteria for increasing over control was 128 at 3 h, 236 at 6 h, and 239 at 9 h. Of the 128 genes increased at 3 h, 95 were in common with those increasing at 6 h, and 53 were in common with the transcripts increasing at 9 h. Of the 236 genes that were increasing at 6 h, 113 were in common with those increasing at 9 h. Of the 53 transcripts that were increased at both 3 and 9 h, 49 were also increased at 6 h. Thus, all but four genes increased at 3 and 9 h were also increased at 6 h (Table 1).

TABLE 1. LIST OF 49 TRANSCRIPTS INCREASED BY 6-OHDA OVER UNTREATED CONTROL AFTER 3, 6, AND 9 H.

		Normalized microarray change (z score)		
Gene symbol	*Gene name*	*3 h*	*6 h*	*9 h*
CHOP/Ddit3	DNA damage-inducible transcript 3	0.38	1.11	2.42
Hmox1	Heme oxygenase 1	0.37	1.24	2.29
Sqstm1	Sequestosome 1	0.44	1.33	2.38
Ubc	Ubiquitin C	0.82	1.02	2.50
Sars1	Seryl-aminoacyl-tRNA synthetase 1	0.94	1.51	2.21
Erdr1	Erythroid differentiation regulator 1	0.96	1.46	2.18
Por	P450 (cytochrome) oxidoreductase	0.55	0.82	2.29
Myd116	Myeloid differentiation primary response gene 116	0.61	1.66	2.21
Nupr1	Nuclear protein 1	1.06	1.63	2.17
Herpud1	Homocysteine-inducible, endoplasmic reticulum stress-inducible, ubiquitin-like domain member 1	1.16	1.55	2.28
Mt2	Metallothionein 2	0.93	1.37	1.91
Gtpbp2	GTP binding protein 2	0.83	1.76	2.21
1810045K07Ril	RIKEN cDNA 1810045K07 gene	0.45	1.23	2.52
Gclm	Glutamate-cysteine ligase, modifier subunit	0.86	1.94	2.05
Jund1	Jun protooncogene-related gene d1	1.30	0.69	2.36
Rnu22	RNA, U22 small nucleolar	1.32	1.94	2.02
Atf4	Activating transcription factor 4	1.45	1.94	1.98
Ier3	Immediate early response 3	1.50	1.21	2.34
Cars	Cysteinyl-tRNA synthetase	1.55	2.18	1.71
Csrp1	Cysteine and glycine-rich protein 1	1.29	1.33	2.35
Psph	Phosphoserine phosphatase	1.55	2.18	1.71
Slc7a5	Solute carrier family 7 (cationic amino acid transporter, y+ system), member 5	1.47	1.56	2.19
Ddr2	Discoidin domain receptor family, member 2	1.24	2.09	1.86
Mthfd2	Methylenetetrahydrofolate dehydrogenase (NAD^+-dependent)	1.76	1.79	1.95
Dusp1	Dual-specificity phosphatase 1	1.61	1.79	2.01
Csrp1	Cysteine and glycine-rich protein 1	1.42	2.16	1.76
1500005G05Ril	RIKEN cDNA 1500005G05 gene	1.32	1.99	1.92
Aars	Alanyl-tRNA synthetase	1.49	2.14	1.77
Slc3a2	Solute carrier family 3 (activators of dibasic and neutral amino acid transport), member 2	1.41	2.05	1.84
5730493B19Ril	RIKEN cDNA 5730493B19Rik	1.95	2.20	1.39
Gas 5	Growth arrest specific 5	1.17	1.56	2.16
Sui1-rs1	Suppressor of initiator codon mutations, related sequence 1 (S. cerevisiae)	1.32	1.60	2.11
Lars	Leucyl-tRNA synthetase	0.91	2.23	1.61
Gdf15	Growth differentiation factor 15	1.57	2.01	1.78
E430001P04Ril	RIKEN cDNA E430001P04 gene	1.53	1.79	1.91
Slc6a9	Solute carrier family 6 (neurotransmitter transporter, glycine), member 9	1.98	2.37	1.16
Tars	Threonyl-tRNA synthetase	1.38	1.53	1.99
Atf3	Activating transcription factor 3	1.80	1.53	2.04
Nfe2l1	Nuclear factor, erythroid-derived 2,-like 1	2.26	1.29	1.68
3110065C23Ril	RIKEN cDNA 3110065C23 gene	1.66	1.81	1.65
Eif4ebp1	Eukaryotic translation initiation factor 4E binding protein 1	1.81	1.96	1.47
Ifld2	Induced in fatty liver dystrophy 2	2.12	1.90	1.41
Cebpb	CCAAT/enhancer binding protein (C/EBP), beta	1.45	1.87	1.48
Clic4/D0Jmb3	Chloride intracellular channel 4/DNA segment, Jeremy M. Boss 3	1.83	1.57	1.28
ArhB	Ras homologue gene family, member B	1.60	2.24	0.59
Slc1a4	Solute carrier family 1 (glutamate/neutral amino acid transporter), member 4	0.50	2.34	0.35
Nars	Asparaginyl-tRNA synthetase	1.82	1.68	0.93
Zfp3612	Zinc finger protein 36, C3H type-like 2	1.33	1.73	0.83
Ddit4	DNA damage-inducible transcript 4	2.17	0.96	0.81

Z score: $z_i = (x_i - x_a)/\sigma$, for the ith value, where x_a = average signal value, and σ = standard deviation.

One way to visualize these temporally complex changes is to plot the induction of genes increasing at one time point versus those increasing at another (Fig. 1). Red horizontal and vertical lines demarcate the threshold set for increasing transcripts (0.5 signal $\log_2$ ratio, ~1.5-fold change). Genes that fall to the right of the vertical red line were increased after 3 h; those falling above the horizontal red line were increased after 6 h (Fig. 1A). Genes in the upper right quadrant were increased at both 3 and 6 h (Fig. 1A). Similarly, data were plotted for genes increasing at 6 versus 9 h and genes increasing at 3 versus 9 h, respectively (Fig. 1B and C). Transcripts increased at all three time points are represented by red closed circles (Fig. 1). In accordance with previous results, these include genes involved in cellular stress responses, signaling, transport, and the ubiquitin-proteasome pathway (Table 1). Similarly, these new data sets confirm and extend our prior findings showing that the stress-induced transcription factor CHOP (Ddit3/Gadd153) is dramatically up-regulated at all time points (Fig. 1, Table 1). Besides CHOP, the genes Atf3, Ifld2, Hmox1, and Sqstm1 are also robustly increased at all three times, whereas Gabarapl1, Armet, and Fkpb11 are increased only at 6 and 9 h (Fig. 1, Table 1).

Another way to compare genes is by their individual signal levels at each time point as opposed to the ratio of their signal levels compared with control. Here signal values are first normalized across experiments via *Z*-scores to make them directly comparable. The subsequent normalized values are used to generate an expression profile for each gene. Data mining software not only allows these expression profiles to be searched for other genes with similar kinetic patterns, but also clusters genes together according to their profiles. Genes identified in Table 1 as increasing at all three time points are ranked according to the correlation of their expression profile with that of CHOP (Gadd153/Ddit3). Therefore, Hmox1 and Sqstm1 have expression profiles closest to CHOP, whereas Slc1a4, Nars, and Ddit4 are the most dissimilar. It should be noted that signal level ranking does not necessarily correlate to fold inductions.

Clustering analysis

Analysis of all genes noted in Table 1 (transcripts increased at all time points) using the K-means clustering algorithm generated three distinct kinetic profiles (Fig. 2). The first, Group 1, are early genes that increase in expression quickly, peaking between 3 and 6 h. Group 2 genes also increase early, but maintain their level of expression, whereas Group 3 genes are generally increasing throughout the time period measured. Overall, most of the gene profiles could be clustered into one of the three subgroups shown in Fig. 2.

Real-time PCR and expression profile comparison

To verify the kinetic profiles and subgroupings identified on the basis of microarray data, we performed real-time PCR analysis on selected genes. Figure 3 compares data generated from real-time PCR experiments (circles and solid lines) with the expression profile generated from the normalized signal values of the microarray (squares and dashed lines). The stress-induced transcription factor CHOP has previously been shown to be up-regulated by 6-OHDA (15). K-means cluster analysis placed CHOP in Group 3 of more slowly rising late genes described above. Figure 3A shows that the microarray profile generated at 3, 6, and 9 h is virtually identical to real-time PCR measurements up to 8 h. Because the microarray

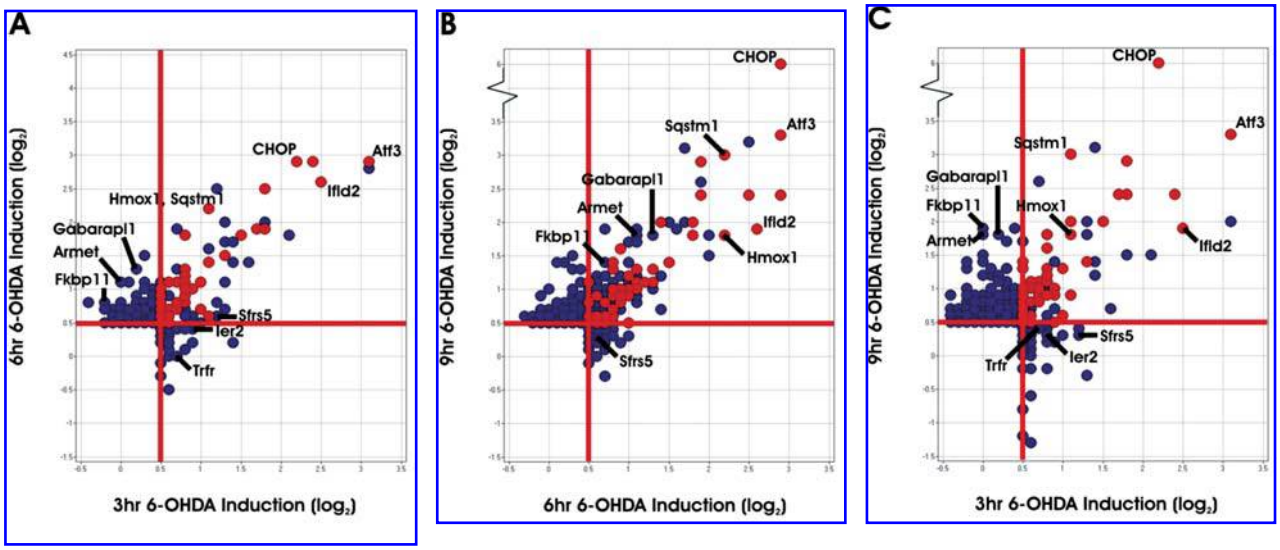

FIG. 1. Kinetic profiling reveals differential gene induction in response to toxin treatment. Total RNA from MN9D cells treated with 6-OHDA or untreated as control was used for Affymetrix MG-U74Av2 GeneChip Array probe hybridization. Data were analyzed by Affymetrix Microarray Suite version 5, as well as Spotfire Decision Site for Functional Genomics. Multiple criteria were defined to identify increasing genes as described in Materials and Methods. (**A**) Genes induced by 6-OHDA at 3 h are plotted against genes induced at 6 h on the *x* axis and *y* axis, respectively, with a scale of $\log_2$. (**B**) Genes induced at 6 h versus genes induced at 9 h. (**C**) Genes induced at 3 h versus those induced at 9 h. Several genes of interest have been labeled (see Table 1 for abbreviations). Solid red lines represent the threshold cutoff of a signal $\log_2$ ratio of 0.5 set to determine increasing genes. Red circles represent genes that met all criteria for determining increasing genes at all three time points. Blue circles represent genes increasing at less than three time points.

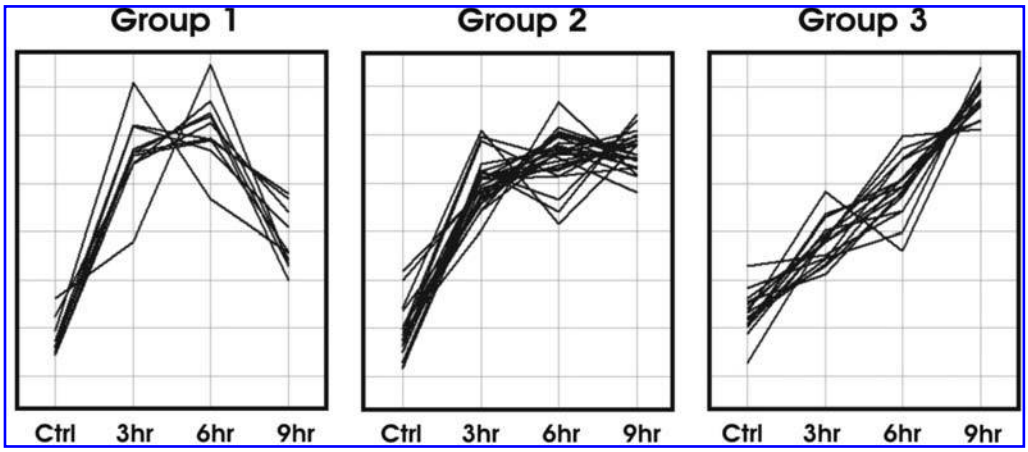

FIG. 2. K-means clustering of increasing genes reveals three distinct expression profiles. Microarray signal values from 51 genes up-regulated at all three time points were normalized by *Z*-score calculation using Spotfire DecisionSite for Functional Genomics. K-means clustering of normalized values was used to generate the three distinct subgroups shown: Group 1, rapid rise and decline; Group 2, rapid rise with plateau; and Group 3, late rise.

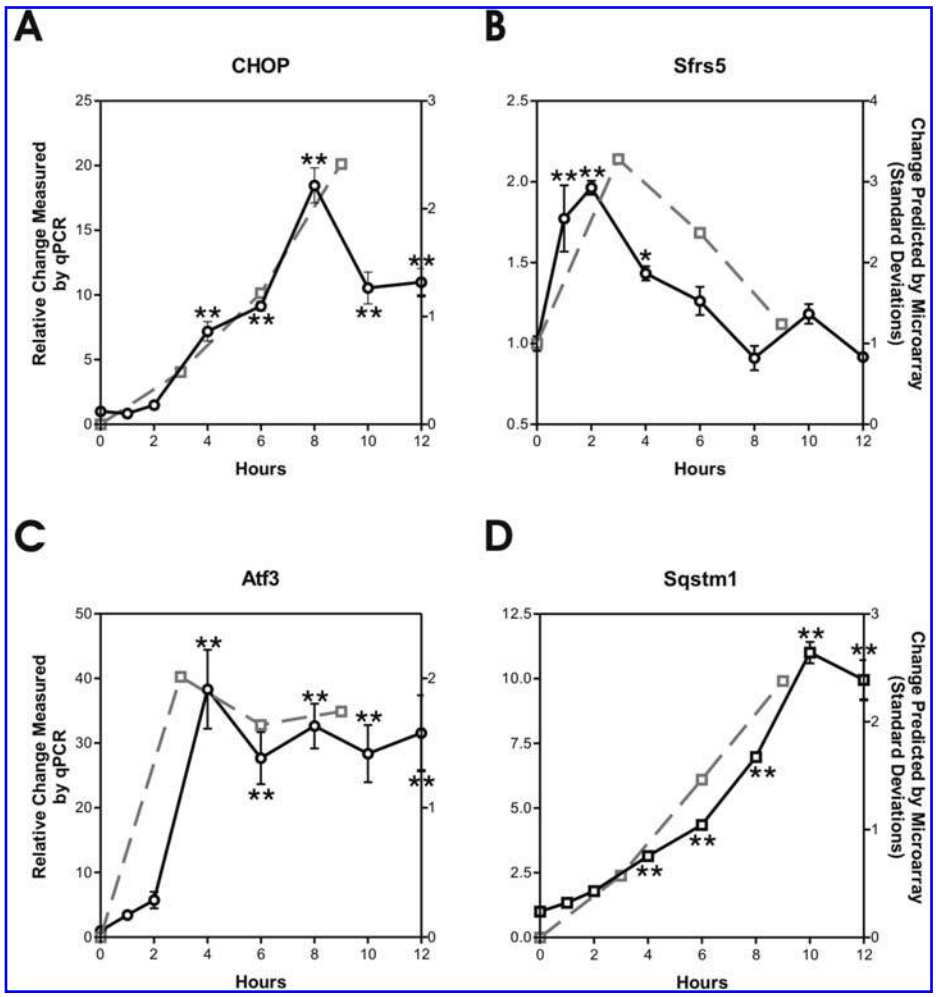

FIG. 3. Real-time PCR confirms microarray expression profiling. Treatment with 6-OHDA increased levels of CHOP, Sfrs5, ATF3, and Sqstm1 as first indicated by microarray analysis and then confirmed by real-time PCR (**A, B, C,** and **D,** respectively). Normalized microarray signal values (see legend of Fig. 2) from control and 3-, 6-, and 9-h time points were plotted to generate a microarray expression profile for genes (squares and dashed lines). Total RNA was isolated from 6-OHDA-treated MN9D cells and used for reverse transcription PCR and real-time PCR analysis using appropriate primers. Input RNA was monitored by measuring GAPDH. Real-time PCR results (circles and solid lines) correspond to their microarray profiles. Values represent means ± SE of three to six replicate real-time PCR reactions. $^{**}p < 0.01$ compared with untreated control (one-way ANOVA with *post-hoc* Dunnett's multiple comparison test). Error bars of < 2% are buried in the symbol.

results do not extend beyond 9 h, they do not predict the decrease observed by real-time PCR at 10 and 12 h. Microarray analysis indicates that the splicing factor, serine/arginine rich 5 (Sfrs5) has a kinetic profile of a gene in Group 1, *i.e.,* genes that peak quickly and then decrease. This early peaking profile was confirmed by real-time PCR results (Fig. 3B). Activating transcription factor 3 (ATF3) was placed by cluster analysis into the group of genes that increased rapidly and remained elevated (Group 2). Real-time PCR corroborates this kinetic profile (Fig. 3C). The gene sequestosome 1 (Sqstm1/p62) was clustered into the same group of late genes as CHOP, because the expression profiles of the two genes were highly correlated (Table 1). This similarity in expression profiles was confirmed by real-time PCR (compare Fig. 3D and A). PCR time points after 9 h, however, reveal that Sqstm1 continues to increase after CHOP levels begin to fall. Taken together, the present microarray results were excellent predictors of *bona fide* transcript responses following toxin treatment.

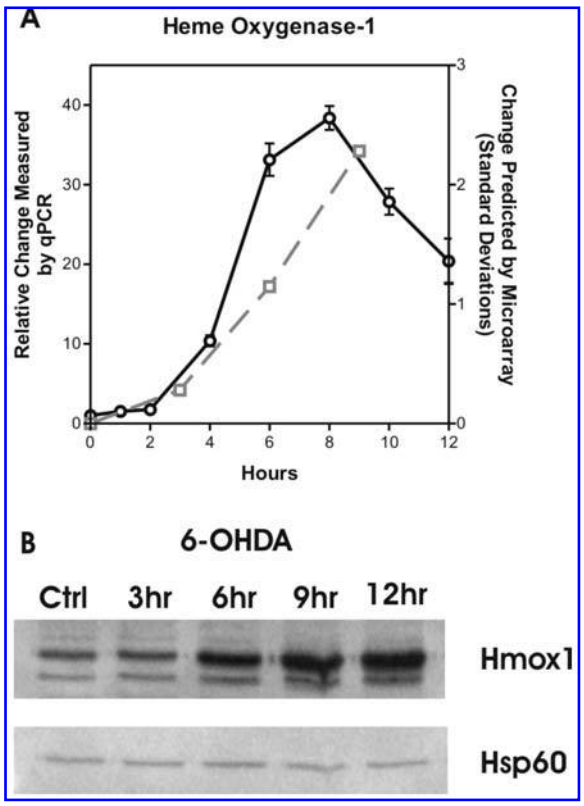

FIG. 4. 6-OHDA induction of Hmox1 can be detected at the mRNA and protein expression levels. (**A**) Normalized microarray signal values were used to generate a microarray expression profile for Hmox1 represented by squares and dashed line. Hmox1 induction measured by real-time PCR (circles and solid line) was similar to the microarray expression profile. (**B**) Protein lysates were prepared from 6-OHDA-treated MN9D cells. Western blot analysis confirmed the up-regulation of Hmox1 protein with a time course of induction consistent with the microarray expression profile and real-time PCR results. Hsp60 western blot is shown as an equal loading control.

Hmox1 induction

Of the genes identified as increasing at all three microarray time points, Hmox1 has an expression profile most closely correlated with CHOP. The Hmox1 kinetic profile was verified via real-time PCR analysis, as well as western blotting of cell lysates from 6-OHDA-treated MN9D cells (Fig. 4). Both RNA and protein patterns indicate that Hmox1 expression parallels that of CHOP.

Two-dimensional gel electrophoresis

With the advent of proteomics, it is possible to examine the consequences of toxin treatment in complex cellular systems. Thus, MN9D cells were treated for 6 h with 6-OHDA alone, 6-OHDA together with the antioxidant NAC, or the dopaminergic toxin MPP^+ alone. Two-dimensional electrophoresis was used to evaluate alterations in the levels of proteins following toxin exposure. Twenty-four proteins showed differential expression, 12 increased and 12 decreased, as a consequence of 6-OHDA treatment (Fig. 5). The majority of these changes were blocked by pretreatment with NAC (data not shown). Of these proteins, CHOP and Hmox1 were further examined by western blotting. Both proteins were barely detectable in untreated control samples, and both were robustly up-regulated in either 6-OHDA- or MPP^+-treated cells. Surprisingly, only CHOP activation was blocked by NAC pretreatment. Hmox1 was less affected (Fig. 5B). Taken together, these data confirm and extend results derived from global genome analysis to the level of the proteome.

DISCUSSION

Functional genomic and proteomic approaches are rapidly becoming valuable tools in deciphering complex regulatory pathways. Building on previous reports showing that cellular stress plays a role in PD (15, 24), the present study identified complex temporal changes associated with aberrant protein degradation following neurotoxin treatment. By analyzing microarray data, distinct functional subgroups of genes were revealed. Notably, stress-induced transcription factors such as ATF3, ATF4, CHOP, and C/EBPβ were all robustly induced, yet exhibited unique kinetic patterns. Multifaceted expression profiles were also observed for genes involved in the synthesis and modification of proteins (*e.g.,* six different tRNA synthetases), protein degradation (*e.g.,* ubiquitin, Herpud1, Sqstm1), oxidative stress (Hmox1, Por), *etc.* Taken together, these data support the notion that oxidative stress and protein dysfunction play a role in PD, as well as provide a time course for many of the molecular events associated with 6-OHDA neurotoxicity.

Clustering of genes involved in 6-OHDA-induced cell death

The ability to group genes based on temporal expression patterns is an important means by which functional relationships or common regulatory mechanisms can be identified. Despite the very large data sets generated from microarray experiments, continually updated algorithms and software

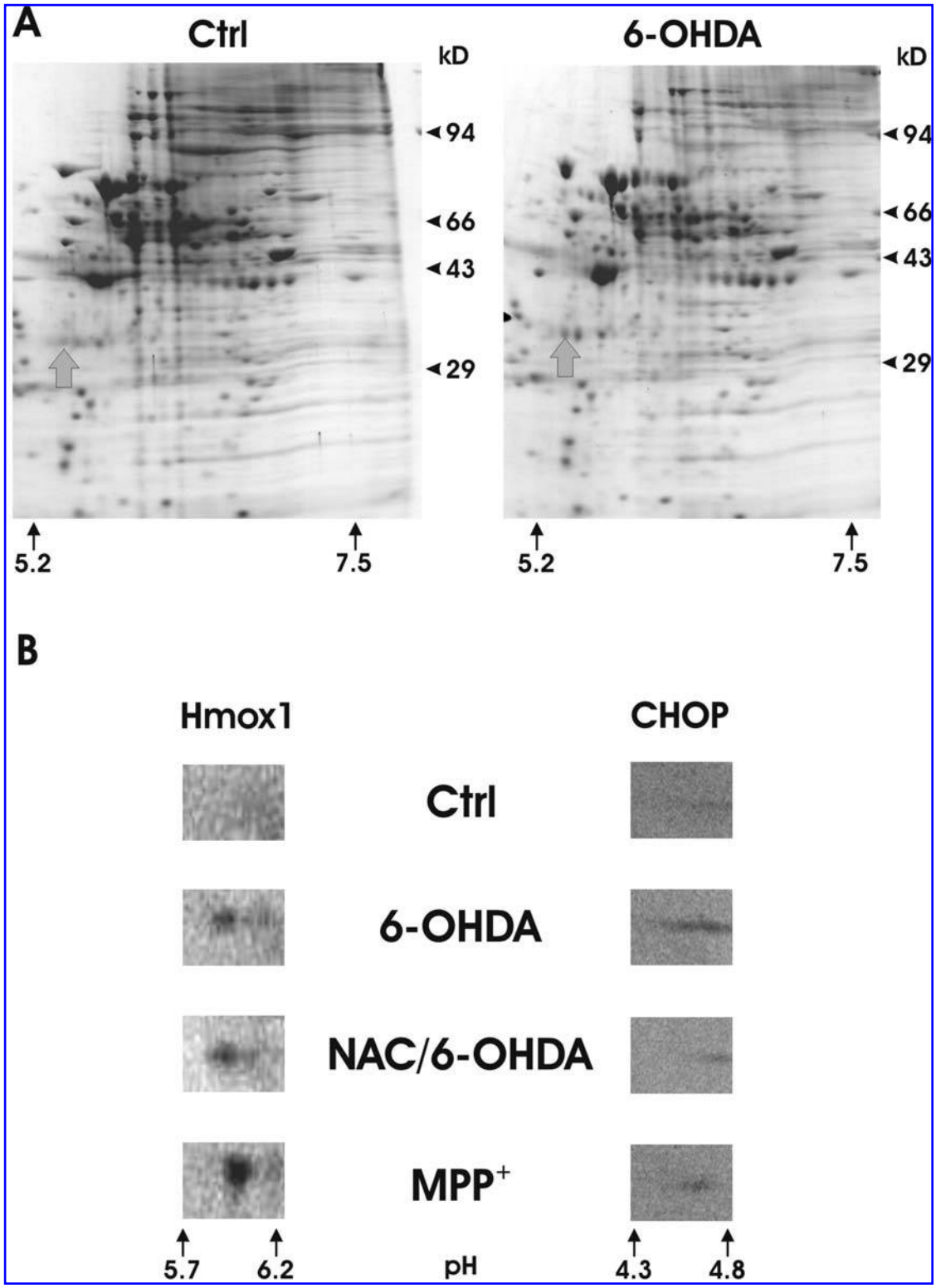

FIG. 5. Two-dimensional gel electrophoresis identifies up-regulation of CHOP and Hmox1 protein levels. MN9D protein lysates from control, 6-OHDA- and MPP^+-treated cells, and cells pretreated with the antioxidant NAC prior to 6-OHDA, were separated by isoelectric focusing followed by SDS-PAGE. Arrowheads denote the position of Hmox1 with a theoretical pI of 6.08 and molecular mass of 32 kDa. Mouse CHOP has a calculated pI of 4.65. Proteins were transferred onto polyvinylidene difluoride membranes for immunoblot detection with anti-Hmox1 or anti-CHOP antibodies.

can be utilized to filter raw information into smaller collections of significance, as well as to cluster transcripts into distinct kinetic profiles. To identify sets of genes of interest, we first filtered genes to single out those that were increasing at each time point. Subsequent comparison of genes induced at one time point against those induced at a different time revealed genes that were distinct to those times, as well as genes that were increased at multiple times (Fig. 1). Genes could be further ranked according to their correlation to a particular gene or profile (22). Because of its large induction, and response to a broad range of insults, we initially focused on the transcription factor CHOP. Genes were ranked according to their kinetic similarity to that of CHOP, which was used as an "anchor" (Table 1). This approach allows for identification of those genes that potentially share functional properties or regulatory elements. By using other genes of interest as anchors, and searching larger data sets for similar expression profiles, *de novo* associations may be discovered.

Application of K-means clustering revealed additional relationships based on shared kinetic pattern profiles, including Group 1 (rapid rise and decline), Group 2 (rapid rise with plateau), and Group 3 (late rise). Conceivably, expression of genes in Groups 1 and 2 may be closely linked to mechanisms that sense cellular changes and thus be required to initiate downstream responses. In contrast, genes in the third group may be involved in either the cell's adaptive response to stress or the execution of a cell death program.

Identification of genes involved in 6-OHDA-induced cell death

The Arg-Ser-rich domain protein, Sfrs5, is a member of a conserved family of splicing factors that can regulate alternative splicing (10). Sfrs5 was identified as an immediate early gene in insulin-treated rat hepatoma H35 cells (9), and identified as a Group 1, rapidly rising, then declining gene, in the current study (Fig. 3B). Several examples exist of alternate mRNA splicing being utilized as a mechanism for regulating stress response. During the unfolded protein response, the endoplasmic reticulum stress sensing protein, Ire1, mediates the unconventional splicing of Xbp1 mRNA to generate an active transcription factor (20, 32). This splicing event has previously been confirmed following 6-OHDA treatment (15). In addition, the stress-induced transcription factor ATF3 (see below) also undergoes stress-induced alternative mRNA splicing to generate truncated isoforms that may modulate the activity of the full-length protein (14, 23). Although Sfrs5 has not been directly implicated in alternative ATF3 splicing, the early profile of this transcript is consistent with a role in regulating downstream events.

Along with CHOP, the transcription factor ATF3 is one of the most highly induced genes (Table 1). Studies have shown that ATF3 is an integral part of the stress cascade, increasing in response to activation of the eIF2 kinases PERK or GCN2, which sense endoplasmic reticulum stress or amino acid starvation, respectively (16). Induction of ATF3 depends on the related bZIP transcription factor ATF4, which was also induced by 6-OHDA exposure. Enhanced levels of ATF4 are achieved via increased transcription, as well as by selective mRNA translation despite the general attenuation of this process (13). Unlike CHOP, whose timing suggests a more downstream role in stress response (compare Fig. 3A and C), early induction of ATF3 is consistent with a more immediate function in the coordination of stress-induced gene expression.

Sqstm1 (p62), a gene encoding a ubiquitin-binding protein, has been shown to be up-regulated during apoptosis and proteasomal inhibition in neuronal cells (17), as well as being localized to inclusion bodies in neurodegenerative disorders such as Alzheimer's disease and PD (17, 18, 33). In SH-SY5Y neuroblastoma and PC12 cell lines, 6-OHDA has been shown to increase the levels of ubiquitin-conjugated proteins (7). Here, Sqstm1 expression was found to rise steadily over 10 h following 6-OHDA treatment (Fig. 3D). This pattern of expression is consistent with Sqstm1 playing a role in the aggregation of accumulating ubiquitinated proteins.

The late expression profile of Hmox1 was similar to that of Sqstm1 (compare Fig. 3D and 4A). Hmox1 has been identified as a component of Lewy body inclusions in PD (27), as well as being induced in response to a wide range of cellular stresses, including oxidative insult of the nigral dopaminergic cell line SN4741 with hydrogen peroxide or MPP^+ (5, 25, 31). Hmox1 functions as an important cellular antioxidant, and an increase in its expression protects against 6-OHDA in PC12 cells (25). As with CHOP and Sqstm1, the timing of Hmox1 induction suggests a downstream role in the stress response, instead of a regulatory role.

Validation of microarray expression profiling

Real-time PCR analysis confirmed that microarray results were predicative of changes for selected genes (Fig. 3). Further, western blot analysis showed that the induction of the gene Hmox1 at the transcript level was consistent with induction of protein levels (Fig. 4). Finally, proteomic analysis via two-dimensional electrophoresis also confirmed up-regulation of Hmox1, as well as the previously identified 6-OHDA-induced stress marker CHOP (Fig. 5). The latter approach has the power to resolve hundreds to thousands of proteins on a single gel. Caveats exist, however. For example, protein preparation using conventional techniques skews results toward hydrophilic proteins. Because cellular stress most likely involves membrane proteins from a variety of sources such as the endoplasmic reticulum, mitochondria, and/or plasma membranes, alternate protein separation techniques may be required to assess complex protein changes following neurotoxin treatments. Present findings indicate that at least 24 proteins are changed in the narrow pI range of 5–8 due to 6-OHDA treatment (Fig. 5 and not shown). Experiments including different pI ranges, as well as native gels (26), will allow assessment of the complete proteome, as well as protein–protein interactions. The latter may be particularly important in the cell's response to stress.

In conclusion, elucidating the biological processes by which parkinsonian mimetics trigger cell death cascades is important to accurately model this disorder. The present findings provide a time frame for molecular events associated with 6-OHDA neurotoxicity and support the role of cellular stress in PD.

ACKNOWLEDGMENTS

We thank Mark Watson and Ting Wang for their insightful comments relating to microarray data interpretation, and Rui Guan and Dillon Paul for their technical assistance. We also thank the Alvin J. Siteman Cancer Center at Washington University School of Medicine and Barnes–Jewish Hospital in St. Louis, Missouri, for the use of the Multiplexed Gene Analysis Core, which provided generation, hybridization, and scanning of target cRNA services. The Siteman Cancer Center is supported, in part, by National Institutes of Health NCI Cancer Center Support Grant P30 CA91842. This work was supported by NIH grant NS39084 and Department of Defense grant DAMD170110777.

ABBREVIATIONS

GAPDH, glyceraldehyde-3-phosphate dehydrogenase; MPP^+, 1-methyl-4-phenylpyridinium; NAC, *N*-acetylcysteine; 6-OHDA, 6-hydroxydopamine; PD, Parkinson's disease; SDS-PAGE, sodium dodecyl sulfate–polyacrylamide gel electrophoresis.

REFERENCES

1. Blum D, Torch S, Lambeng N, Nissou M, Benabid AL, Sadoul R, and Verna JM. Molecular pathways involved in the neurotoxicity of 6-OHDA, dopamine and MPTP: contribution to the apoptotic theory in Parkinson's disease. *Prog Neurobiol* 65:135–172, 2001.
2. Choi HK, Won LA, Kontur PJ, Hammond DN, Fox AP, Wainer BH, Hoffmann PC, and Heller A. Immortalization of embryonic mesencephalic dopaminergic neurons by somatic cell fusion. *Brain Res* 552: 67–76, 1991.
3. Choi W-S, Canzoniero LMT, Sensi SL, O'Malley KL, Gwag BJ, Sohn S, Kim J-E, Oh TH, Lee EB, and Oh YJ. Characterization of MPP^+-induced cell death in a dopaminergic neuronal cell line: role of macromolecule synthesis, cytosolic calcium, caspase, and Bcl-2-related proteins. *Exp Neurol* 159: 274–282, 1999.
4. Choi W-S, Yoon S-Y, Oh TH, Choi E-J, O'Malley KL, and Oh YJ. Two distinct mechanisms are involved in 6-hydroxydopamine- and MPP^+-induced dopaminergic neuronal cell death: role of caspases, ROS, and JNK. *J Neurosci Res* 57: 86–94, 1999.
5. Chun HS, Gibson GE, DeGiorgio LA, Zhang H, Kidd VJ, and Son JH. Dopaminergic cell death induced by MPP^+, oxidant and specific neurotoxicants shares the common molecular mechanism. *J Neurochem* 76: 1010–1021, 2001.
6. Curtius HC, Wolfensberger M, Steinmann B, Redweik U, and Siegfried J. Mass fragmentography of dopamine and 6-hydroxydopamine. Application to the determination of dopamine in human brain biopsies from the caudate nucleus. *J Chromatogr* 99: 529–540, 1974.
7. Dawson T, Mandir A, and Lee M. Animal models of PD: pieces of the same puzzle? *Neuron* 35: 219–222, 2002.
8. Dawson TM and Dawson VL. Molecular pathways of neurodegeneration in Parkinson's disease. *Science* 302: 819–822, 2003.
9. Diamond RH, Du K, Lee VM, Mohn KL, Haber BA, Tewari DS, and Taub R. Novel delayed-early and highly insulin-induced growth response genes. Identification of HRS, a potential regulator of alternative pre-mRNA splicing. *J Biol Chem* 268: 15185–15192, 1993.
10. Du K, Leu JI, Peng Y, and Taub R. Transcriptional upregulation of the delayed early gene HRS/SRp40 during liver regeneration. Interactions among YY1, GA-binding proteins, and mitogenic signals. *J Biol Chem* 273: 35208–35215, 1998.
11. Fornstedt B, Rosengren E, and Carlsson A. Occurrence and distribution of 5-*S*-cysteinyl derivatives of dopamine, dopa and dopac in the brains of eight mammalian species. *Neuropharmacology* 25: 451–454, 1986.
12. Han BS, Hong HS, Choi WS, Markelonis GJ, Oh TH, and Oh YJ. Caspase-dependent and -independent cell death pathways in primary cultures of mesencephalic dopaminergic neurons after neurotoxin treatment. *J Neurosci* 23: 5069–5078, 2003.
13. Harding HP, Zhang Y, Zeng H, Novoa I, Lu PD, Calfon M, Sadri N, Yun C, Popko B, Paules R, Stojdl DF, Bell JC, Hettmann T, Leiden JM, and Ron D. An integrated stress response regulates amino acid metabolism and resistance to oxidative stress. *Mol Cell* 11: 619–633, 2003.
14. Hashimoto Y, Zhang C, Kawauchi J, Imoto I, Adachi MT, Inazawa J, Amagasa T, Hai T, and Kitajima S. An alternatively spliced isoform of transcriptional repressor ATF3 and its induction by stress stimuli. *Nucleic Acids Res* 30: 2398–2406, 2002.
15. Holtz WA and O'Malley KL. Parkinsonian mimetics induce aspects of unfolded protein response in death of dopaminergic neurons. *J Biol Chem* 278: 19367–19377, 2003.
16. Jiang HY, Wek SA, McGrath BC, Lu D, Hai T, Harding HP, Wang X, Ron D, Cavener DR, and Wek RC. Activating transcription factor 3 is integral to the eukaryotic initiation factor 2 kinase stress response. *Mol Cell Biol* 24: 1365–1377, 2004.
17. Kuusisto E, Suuronen T, and Salminen A. Ubiquitin-binding protein p62 expression is induced during apoptosis and proteasomal inhibition in neuronal cells. *Biochem Biophys Res Commun* 280: 223–228, 2001.
18. Kuusisto E, Parkkinen L, and Alafuzoff I. Morphogenesis of Lewy bodies: dissimilar incorporation of alpha-synuclein, ubiquitin, and p62. *J Neuropathol Exp Neurol* 62: 1241–1253, 2003.
19. Lansbury PT Jr and Brice A. Genetics of Parkinson's disease and biochemical studies of implicated gene products. *Curr Opin Cell Biol* 14: 653–660, 2002.
20. Lee K, Tirasophon W, Shen X, Michalak M, Prywes R, Okada T, Yoshida H, Mori K, and Kaufman RJ. IRE1-mediated unconventional mRNA splicing and S2P-mediated ATF6 cleavage merge to regulate XBP1 in signaling the unfolded protein response. *Genes Dev* 16: 452–466, 2002.
21. Morrison TB, Weis JJ, and Wittwer CT. Quantification of low-copy transcripts by continuous SYBR Green I monitoring during amplification. *Biotechniques* 24: 954–958, 960, 962, 1998.

22. Nagarajan R, Le N, Mahoney H, Araki T, and Milbrandt J. Deciphering peripheral nerve myelination by using Schwann cell expression profiling. *Proc Natl Acad Sci U S A* 99: 8998–9003, 2002.
23. Pan Y, Chen H, Siu F, and Kilberg MS. Amino acid deprivation and endoplasmic reticulum stress induce expression of multiple activating transcription factor-3 mRNA species that, when overexpressed in HepG2 cells, modulate transcription by the human asparagine synthetase promoter. *J Biol Chem* 278: 38402–38412, 2003.
24. Ryu EJ, Harding HP, Angelastro JM, Vitolo OV, Ron D, and Greene LA. Endoplasmic reticulum stress and the unfolded protein response in cellular models of Parkinson's disease. *J Neurosci* 22: 10690–10698, 2002.
25. Salinas M, Diaz R, Abraham NG, Ruiz de Galarreta CM, and Cuadrado A. Nerve growth factor protects against 6-hydroxydopamine-induced oxidative stress by increasing expression of heme oxygenase-1 in a phosphatidylinositol 3-kinase-dependent manner. *J Biol Chem* 278: 13898–13904, 2003.
26. Schagger H and von Jagow G. Blue native electrophoresis for isolation of membrane protein complexes in enzymatically active form. *Anal Biochem* 199: 223–231, 1991.
27. Schipper HM, Liberman A, and Stopa EG. Neural heme oxygenase-1 expression in idiopathic Parkinson's disease. *Exp Neurol* 150: 60–68, 1998.
28. Siderowf A and Stern M. Update on Parkinson disease. *Ann Intern Med* 138: 651–658, 2003.
29. Spencer JP, Jenner P, Daniel SE, Lees AJ, Marsden DC, and Halliwell B. Conjugates of catecholamines with cysteine and GSH in Parkinson's disease: possible mechanisms of formation involving reactive oxygen species. *J Neurochem* 71: 2112–2122, 1998.
30. Stokes AH, Hastings TG, and Vrana KE. Cytotoxic and genotoxic potential of dopamine. *J Neurosci Res* 55: 659–665, 1999.
31. Yoo MS, Chun HS, Son JJ, DeGiorgio LA, Kim DJ, Peng C, and Son JH. Oxidative stress regulated genes in nigral dopaminergic neuronal cells: correlation with the known pathology in Parkinson's disease. *Brain Res Mol Brain Res* 110: 76–84, 2003.
32. Yoshida H, Matsui T, Yamamoto A, Okada T, and Mori K. XBP1 mRNA is induced by ATF6 and spliced by IRE1 in response to ER stress to produce a highly active transcription factor. *Cell* 107: 881–891, 2001.
33. Zatloukal K, Stumptner C, Fuchsbichler A, Heid H, Schnoelzer M, Kenner L, Kleinert R, Prinz M, Aguzzi A, and Denk H. p62 is a common component of cytoplasmic inclusions in protein aggregation diseases. *Am J Pathol* 160: 255–263, 2002.

Address reprint requests to:
Karen O'Malley, Ph.D.
Washington University School of Medicine
Anatomy and Neurobiology Department Box 8108
660 South Euclid Ave.
St. Louis, MO 63110

E-mail: omalleyk@pcg.wustl.edu

Received for publication October 5, 2004; accepted November 30, 2004.

This article has been cited by:

1. Bokyung Park, Chang-Ki Oh, Won-Seok Choi, In Kwon Chung, Moussa B. H. Youdim, Young J. Oh. 2011. Microarray expression profiling in 6-hydroxydopamine-induced dopaminergic neuronal cell death. *Journal of Neural Transmission* . [CrossRef]
2. Sang J. Na, Anthony G. DiLella, Edward V. Lis, Keith Jones, David M. Levine, David J. Stone, J. F. Hess. 2010. Molecular Profiling of a 6-Hydroxydopamine Model of Parkinson's Disease. *Neurochemical Research* **35**:5, 761-772. [CrossRef]
3. Päivi Lindholm, Mart Saarma. 2010. Novel CDNF/MANF family of neurotrophic factors. *Developmental Neurobiology* NA-NA. [CrossRef]
4. Jeong Sook Kim-Han , Karen L. O'Malley . 2007. Cell Stress Induced by the Parkinsonian Mimetic, 6-Hydroxydopamine, is Concurrent with Oxidation of the Chaperone, ERp57, and Aggresome Formation. *Antioxidants & Redox Signaling* **9**:12, 2255-2264. [Abstract] [Full Text PDF] [Full Text PDF with Links]
5. William A. Holtz, Jay M. Turetzky, Yuh-Jiin I. Jong, Karen L. O'Malley. 2006. Oxidative stress-triggered unfolded protein response is upstream of intrinsic cell death evoked by parkinsonian mimetics. *Journal of Neurochemistry* **99**:1, 54-69. [CrossRef]
6. Todd B. Sherer , J. Timothy Greenamyre . 2005. Oxidative Damage in Parkinson's Disease. *Antioxidants & Redox Signaling* **7**:5-6, 627-629. [Citation] [Full Text PDF] [Full Text PDF with Links]